molecular pharmaceutics

pubs.acs.org/molecularpharmaceutics

Article

Oral Lipid-Based Nanomedicine for the Inhibition of the cGAS-STING Pathway in Inflammatory Bowel Disease Treatment

Published as part of Molecular Pharmaceutics special issue "Pharmaceutical Sciences and Drug Delivery Research from Early Career Scientists".

Léo Guilbaud, Cheng Chen, Inês Domingues, Espoir K. Kavungere, Valentina Marotti, Hafsa Yagoubi, Wunan Zhang, Alessio Malfanti,* and Ana Beloqui*

Cite This: *Mol. Pharmaceutics* 2025, 22, 2108−2121

Read Online

ACCESS | Metrics & More | Article Recommendations | Supporting Information

ABSTRACT: Harnessing the effect of the cyclic GMP-AMP Synthase-STimulator of INterferon Genes (cGAS-STING) signaling pathway has emerged as a promising approach to developing novel strategies for the oral treatment of inflammatory bowel disease (IBD). In this work, we screened different cGAS-STING inhibitors *in vitro* in murine macrophages. Then, we encapsulated the cGAS-STING inhibitor H-151 within lipid nanocapsules (LNCs), owing to their inherent ability to induce the secretion of glucagon-like peptide 2 (GLP-2), a re-epithelizing peptide, upon oral administration. We demonstrated that our formulation (LNC(H-151)) could induce GLP-2 secretion and selectively target the cGAS-STING pathway and its downstream key markers (including TBK1 and pTBK1) while reducing the expression of pro-inflammatory cytokines associated with the cGAS-STING pathway (TNF-α and CXCL10) in murine macrophages. In an *in vivo* acute dextran sodium sulfate (DSS)-induced colitis mouse model, the oral administration of LNC(H-151) significantly reduced pro-inflammatory cytokines to levels comparable to the CTRL Healthy group while promoting mucosal healing. The therapeutic potential of this scalable and cost-effective nanomedicine warrants further investigation as an alternative for the oral treatment of IBD.

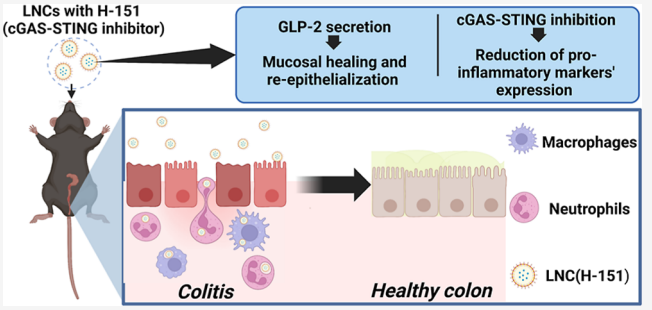

KEYWORDS: *inflammatory bowel disease, cGAS-STING pathway, lipid nanocapsules, GLP-2 secretion, mucosal healing, re-epithelialization*

1. INTRODUCTION

Inflammatory bowel disease (IBD) is a chronic autoimmune disease characterized by relapsing-remitting episodes and it presents two main forms: ulcerative colitis (UC) and Crohn's disease (CD). The condition manifests symptoms such as diarrhea, abdominal pain, rectal bleeding, and weight loss, necessitating lifelong chronic administration of anti-inflammatory therapies.[1−4] The pathogenesis of IBD is intricately linked to an unbalanced intestinal immune response.[5] Exposure of the gastrointestinal (GI) mucosa to diverse microbial populations might lead to GI inflammation and potential malignancies (e.g., cancer).[6]

Currently, the treatment for IBD consists of a combination of different therapeutic strategies depending on the severity of the disease. These involve the use of immunomodulators (e.g., thiopurines, methotrexate, and calcineurin inhibitors), aminosalicylates, and corticosteroids as first-line treatments.[7] These approaches can be further complemented with monoclonal antibodies such as antitumor necrosis factor-alpha (TNF-α), anti-integrin, and anti-interleukin (IL)-12 and IL-23 antibodies. Additionally, surgical procedures can be performed depending on the severity and location of the disease.[2,7,8] However, current strategies fail to improve the quality of life of patients suffering from this debilitating disorder.

Intestinal macrophages and neutrophils are innate immune cells that orchestrate the alteration of intestinal epithelial barrier function and play important roles in the imbalance of immune homeostasis in IBD.[9] One of the drivers of the inflammatory response of these innate cells in IBD is the cyclic Guanosine monophosphate-Adenosine monophosphate Synthase-STimulator of INterferon Genes (cGAS-STING) pathway.[10] cGAS is an intracellular DNA sensor that regulates innate immunity by forming cyclic guanosine monophosphate-

Received: November 5, 2024
Revised: February 17, 2025
Accepted: February 18, 2025
Published: March 3, 2025

adenosine monophosphate (cGAMP) and activating STING downstream, thus activating type I interferon (IFN) and other pro-inflammatory cytokines/chemokines (e.g., TNF-α, CXCL10, MIP-1α) via nuclear factor-κB (NF-κB) and TANK-binding kinase 1 (TBK1).[6,11−13] Recent studies have highlighted the role of the cGAS-STING pathway in autoimmune intestinal disorders and GI homeostasis, suggesting its potential as a therapeutic target for IBD, as reported in a recent clinical trial (NCT05916274).[6,10,14]

Although the cGAS-STING pathway represents a druggable site for decreasing the inflammatory state during IBD, one of the main limitations in the development of cGAS-STING inhibitor-based therapies is related to the biopharmaceutical properties of the inhibitors (e.g., high lipophilicity) and the need for intracellular delivery to target the cGAS-STING pathway. In addition, the low bioavailability and degradation of these drugs in GI fluids can be particularly challenging in the context of oral delivery for IBD treatment. Previously, the murine cGAS inhibitor RU.521 was encapsulated in polymeric micelles that were designed for targeted drug release in the inflamed colon upon oral administration. These micelles exhibited promising results comparable to those of 5-aminosalicylic acid (5-ASA) in an ulcerative colitis model.[15]

In this work, we investigated the use of three different cGAS-STING inhibitors, namely, SN-011, C-176, and H-151. By comparing the effects of these different inhibitors and their mechanisms of action, we sought to investigate which inhibitor would be the most promising for inhibiting the cGAS-STING pathway in macrophages. Next, we hypothesized that an oral nanoparticle-based formulation for the encapsulation of lipophilic cGAS-STING inhibitors based on lipid nanocapsules (LNCs) would represent a promising strategy for the clinical translation of cGAS-STING inhibitors in IBD treatment. LNCs are well-known for their biocompatibility and nonimmunogenicity and have demonstrated high drug encapsulation capacity for poorly water-soluble drugs, improved drug solubility, protection of the drug from degradation in the GI tract, and enhanced bioavailability.[16,17] Additionally, recent findings revealed an intrinsic effect of oral LNCs administration on increased GLP-2 secretion.[1] Hence, in this study, we focused on the use of LNCs as an oral cGAS-STING inhibitor nanocarrier in an acute dextran sodium sulfate (DSS)-induced colitis mouse model. The efficacy of the final formulation was evaluated based on its ability to reduce colonic inflammation via cGAS-STING pathway inhibition while promoting the re-epithelialization of the intestinal mucosa via GLP-2 secretion.

2. MATERIALS AND METHODS

2.1. Materials. 2′3′cGAMP (cGAMP, STING agonist) was purchased from InvivoGen (San Diego, CA, USA). SN-011 and C-176 were purchased from Selleckchem (Houston, TX, USA). H-151 was purchased from MedChemExpress (South Brunswick, NJ, USA). Labrafac WL 1349 (caprylic/capric acid triglycerides) and Peceol (oleic acid mono-, di- and triglycerides) were kindly provided by Gattefossé (Saint-Priest, France). Lipoid S100 (soybean lecithin at 94% of phosphatidylcholines) was a gift from Lipoid GmbH (Ludwigshafen, Germany). Kolliphor HS15 (12-hydroxystearate PEG 660) Tween 80 (polysorbate), Tween20, sodium deoxycholic acid, Tris−HCl, *o*-dianisidine, hexadecyltrimethylammonium bromide (HTAB) and sodium chloride (NaCl) were purchased from Sigma-Aldrich (St. Louis, MO, USA). Dextran sulfate sodium (DSS) (M_w ∼ 40 kDa) was purchased from TdB Consultancy (Uppsala, Sweden). Dulbecco's phosphate-buffered saline (DPBS), Roswell Park Memorial Institute −1640 (RPMI 1640), RPMI-1640 + GlutaMAX medium, Dubelcco's Modified Eagle Medium (DMEM), inactivated fetal bovine serum (FBS), penicillin/streptomycin, ethylenediaminetetraacetic acid (EDTA), Nonidet P40 Substitute (NP-40), Page Ruler plus retained protein ladder 10−250 kDa, Lane marker Reducing sample buffer (5×), SuperSignal West Pico Plus chemiluminescent substrate and SuperSignal West Femto Maximum Sensitivity Substrate were purchased from Thermo Fisher Scientific (Waltham, MA, USA). Protease inhibitor cocktail tablets (Complete Mini, EDTA-free) and phosphatase inhibitor cocktail tablets (PhosSTOP EASY Pack) were purchased from Roche Diagnostics (Basel, Switzerland). Triton X-100, dimethyl sulfoxide (DMSO), and ROTI Histofix 4% formaldehyde solution (pH = 7) were purchased from Carl Roth GmbH (Karlsruhe, Germany). Sodium dodecyl sulfate (SDS) was purchased from Bio-Rad (Hercules, CA, USA). Potassium dihydrogen phosphate and hydrogen peroxide were obtained from Merck (Darmstadt, Germany). 15-well acrylamide gels with gradients of 4−15%, polyvinylidene fluoride (PVDF) membranes, extra thick blotting paper, TRIS/Glycine/SDS buffer and TRIS/Glycine buffer were purchased from Bio-Rad (Hercules, CA, USA). Protease-free albumin bovine serum (BSA) was purchased from VWR (Radnor, PA, USA). Tris-buffered saline (10×, TBS) was purchased from ChemCruz (Santa Cruz Biotechnology, Santa Cruz, CA, USA). Dipeptidyl peptidase 4 (DPP-IV) inhibitor was purchased from Millipore (Burlington, MA, USA). All chemical reagents used in this study were of analytical grade.

2.2. Methods. *2.2.1. Preparation and Characterization of Lipid Nanocapsules (LNCs).* LNCs were prepared by using the phase inversion process first described by Heurtault et al.,[18] with slight modifications. Labrafac WL 1349, Peceol, Kolliphor HS15, Lipoid, and H-151 were dissolved in acetone (300 μL). After acetone removal by evaporation, an aqueous solution of NaCl (5% w/w) was added to the mixture. Next, five cycles (from 48 to 70 °C) of progressive heating/cooling were performed under constant stirring (300 rpm). Cold Milli-Q water (4 °C) was added during the last cooling step at 60.5 °C. Blank LNCs were prepared by following the same protocol without the drug. The resulting LNCs were then stored at 4 °C until use. The final formulation compositions are summarized in Table S1.

2.2.2. Drug Loading and Encapsulation Efficiency. LNCs loaded with H-151 [referred to as LNC(H-151)] were diluted in methanol (dilution factor of 1/20). Free and encapsulated H-151 were separated by ultrafiltration using Amicon centrifuge filters (cut off = 100 kDa, Millipore, Burlington, MA, USA) and quantified by high-performance liquid chromatography (HPLC, Shimadzu, Japan) using a Nucleodur C18 column (125 × 4.6 mm) (Macherey-Nagel, Düren, Germany). Water supplemented with trifluoroacetic acid (0.05%, eluent A) and acetonitrile (eluent B) was used as the mobile phase in gradient mode (95% A and 5% B at 0 min; 5% A and 95% B at 9 min; 5% A and 95% B at 11 min; 95% A and 5% B at 12 min; 95% A and 5% B at 13 min). The flow rate was set at 1 mL/min. Drug detection was performed using a UV detector set at a wavelength of 230 nm. The total and free drug contents were assessed through a calibration curve with H-151 (concentration range of 5−100 μg/mL; R^2 = 0.99; H-151 retention time: 6.9 min; limit of detection (LOD): 1.8 ± 0.4 μg/mL; limit of quantification (LOQ): 5.4 ± 1.2 μg/

https://doi.org/10.1021/acs.molpharmaceut.4c01297
Mol. Pharmaceutics 2025, 22, 2108−2121

mL). The encapsulation efficiency (EE) and drug loading (DL) were then quantified following the eqs 1 and 2

$$\mathrm{EE} = \frac{\text{total drug} - \text{free drug}}{\text{total drug}} \times 100[\%] \quad (1)$$

$$\mathrm{DL} = \frac{\text{total drug} - \text{free drug}}{\text{weighted Labrafac}} \times 100[\%] \quad (2)$$

2.2.3. Physicochemical Characterization. The pK_a values of the different inhibitors were calculated using the software *Chemicalize* (Chemaxon, Budapest, Hungary).

The LNCs were characterized in terms of size, polydispersity index (PdI) and zeta potential using a Zetasizer Ultra (Malvern Instruments Ltd., Worcestershire, U.K.). Each formulation was measured five times (10 μL of LNCs in 2.0 mL of ultrapure water), with three replicates. The formulation stability at 4 °C was assessed on days 0, 30, and 90.

2.2.4. In Vitro Stability Studies and Drug Release in Simulated Gastric, Intestinal and Colonic Fluids. The *in vitro* stability of LNC(H-151) was tested in 3 different biomimetic media: fasted state-simulated gastric fluid (FASSGF), fasted state-simulated intestinal fluid version 2 (FASSIF), fasted state-simulated intestinal fluid (FASSCOF) (Biorelevant, London, U.K., except for FASSGF). A detailed description of the composition of the simulated fluids used is depicted in Table S2. The influence of gastric, intestinal, and colonic conditions on LNCs' stability was evaluated with the size, PdI and nanoparticle concentration using a Zetasizer Ultra (Malvern Instruments Ltd., Worcestershire, U.K.). LNC(H-151) were incubated in the different media at 37 °C (100 μL of nanocapsules in 4.9 mL of media) under gentle stirring. At predetermined time intervals (0, 0.5, 1, 2, 3, and 6 h), 250 μL of the solution were withdrawn, diluted with 750 μL of the corresponding medium (FASSGF, FASSIF, and FASSCOF) and then analyzed by DLS.

The drug release protocol was adapted from previous drug release studies with LNCs.[19,20] To maintain sufficient solubility conditions for H-151 into the mediums, FASSGF, FASSIF, and FASSCOF were complemented with 1% (v/v) Tween 80. The drug release was performed in an incubator at 37 °C and constantly shaken at a speed of 100 rpm. A volume of 1 mL of LNC(H-151) (equivalent of ∼5.4 mg of H-151) was placed in a dialysis tube (Float-A-Lyzer G2, MW:3.5−5 kDa) (Repligen, Waltham, MA, USA). The dialysis tube was immersed in a container with 25 mL of FASSGF. Aliquots of 0.5 mL were withdrawn from the container solution at 0, 0.5, 1, and 2 h and replaced with the same volume of FASSGF. After 2 h, the dialysis tube was transferred to another container with 25 mL of FASSIF. Aliquots of 0.5 mL were withdrawn from the container solution at 0, 0.5, 1, 2, and 3 h and replaced with the same volume of FASSIF. Then, the dialysis tube was placed into a container with 25 mL of FASSCOF. Aliquots of 0.5 mL were withdrawn from the container solution at 0, 0.5, 1, 2, 3, 6, 12, and 24 h and replaced with the same volume of FASSCOF. All the aliquots were mixed with 0.5 mL of methanol and H-151 was further quantified using HPLC. The amount of H-151 released was quantified using a standard curve in each simulated GI fluid. The cumulative drug release from LNCs was determined by the following eq 3

$$\text{cumulative drug release} = \frac{\text{drug quantified in medium}}{\text{theoretical drug amount within nanocapsules}} \times 100[\%] \quad (3)$$

2.2.5. In Vitro Cell Studies. 2.2.5.1. Cell Cultures. The intestinal murine L cell line GLUTag was kindly provided by Prof. Daniel J. Drucker (University of Toronto, Canada). The cells were grown in DMEM supplemented with 10% (v/v) inactivated FBS and 1% (v/v) penicillin/streptomycin (complete DMEM) at 37 °C in a 5% CO_2 atmosphere.

J774 cells (murine macrophages) (American Type Culture Collection, ATCC, Manassas, VA, USA) were grown in RPMI-1640 with L-glutamine supplemented with 10% (v/v) inactivated FBS and 1% (v/v) penicillin/streptomycin at 37 °C in a 5% CO_2 atmosphere.

Primary intraperitoneal (IP) macrophages were harvested from C57BL/6J mice as adapted from Alhouayek et al.[21] IP macrophages were cultured at 37 °C in 5% CO_2 using RPMI-1640 + GlutaMAX supplemented with 10% (v/v) inactivated FBS and 1% (v/v) penicillin/streptomycin. Sterile ice-cold PBS (6 mL) was injected into the IP cavity of the sacrificed mice using a 26G needle. The syringe wound was blocked using forceps while the mixture was agitated to detach the macrophages from the IP cavity. The macrophages were then extracted using an 18G sterile needle and pooled into 50 mL conical Falcon tubes. Next, the cell suspension was centrifuged, and the pellet was resuspended in the medium. After 3 h, the cells were washed three times with PBS to remove non-macrophage cells and debris. IP-purified macrophages were used and treated for the experiment directly after being washed with PBS.

2.2.5.2. Real-Time Quantitative Polymerase Chain Reaction (RT-qPCR). mRNA extraction and isolation were performed following the TRIzol Reagent user guide (Thermo Fisher Scientific, Waltham, MA, USA). mRNA isolation was performed by adding 200 μL of TRIzol reagent and 40 μL of chloroform per sample. Next, the lysed cells were centrifuged at 12,000*g* for 15 min at 4 °C. mRNA was isolated using isopropanol, then 75% ethanol (v/v), and finally, it was dissolved in 10 μL of endotoxin-free Tris−EDTA (TE) buffer (ultrapure water with 10 mM Tris and 1 mM EDTA, pH ∼ 8.0). The total mRNA concentration (ng/mL) and purity were assessed using a Nanodrop 2000 spectrophotometer (Thermo Fisher Scientific, Waltham, MA, USA). The mRNA (0.33 μg/μL in TE buffer) was reverse transcribed using GoScript Reverse Transcription Mix, Oligo(dT) (Promega, Madison, WI, USA). qPCR was performed by using GoTaq qPCR Master Mix (primer sequences reported in Table S3) with a QIAquant 96 2 plex (QIAGEN, Netherlands). Relative expression analysis was normalized against RPL19 as a reference gene, and the relative expression level was calculated using the comparative ($2^{-\Delta\Delta CT}$) method.

2.2.5.3. Drug Screening Assay. J774 cells (2×10^5 cells/well) were seeded in 24-well plates. After 24 h, the cells were treated with 0.5 μM of the following cGAS-STING inhibitors: SN-011, C-176, and H-151 for 1 h. Following this incubation period, the cells were challenged with cGAMP (1.5 μg/mL) or lipopolysaccharides (LPS) (1 μg/mL) for 5 h. After that, the supernatant was removed, and the mRNA was extracted from the cells and further processed by RT-qPCR using the method described above. Cells treated with DMSO/medium (equiv-

https://doi.org/10.1021/acs.molpharmaceut.4c01297
Mol. Pharmaceutics 2025, 22, 2108−2121

alent concentration as per the inhibitor solution), cGAMP- or LPS-activated cells, and untreated cells (CTRL) were used as controls.

2.2.5.4. Cell Viability Assay. J774 cells (2×10^5 cells/well) were seeded onto 96-well plates. After 24 h, the cells were treated with H-151 (0.0001−1 μM) or LNC(H-151) (0.0001−1 μM H-151) and coincubated for 24 h. Then, the cells were fixed with 100 μL of PFA (4% v/v in water) for 30 min. PFA was removed by aspiration, and the cells were treated with 100 μL of crystal violet (CV, Millipore, Burlington, MA, USA) stain [500 mg of CV diluted in 100 mL (80:20, water/MeOH)]. The cells were then incubated at room temperature for 30 min and subsequently washed three times with 300 μL of ultrapure water and dried for 1 h at room temperature. Lastly, the CV crystals were resolubilized with 100 μL of methanol and shaken for 30 min. The absorbance (λ = 560 nm) was measured with a SpectraMax ID5 instrument (Molecular Devices, San Jose, CA, USA). The untreated group was considered 100% cell viability.

2.2.5.5. GLP-2 Secretion Study in Murine GLUTag Cells. For the secretory studies, GLUTag cells (1.8×10^5 cells/well) were seeded onto 24-well Matrigel-coated (10 μL/mL of medium) cell culture plates and allowed to adhere for 24 h. The next day, the cells were treated with LNC(H-151) for 2 h. The nanoparticle concentration (2 mg/mL of LNCs) was selected on the basis of previous studies.[1,22] All the experiments were conducted in complete DMEM supplemented with DPP-IV inhibitor at a final concentration of 50 μM. Total GLP-2 concentrations were determined with an ELISA kit from Crystal Chem Inc. (Elk Grove Village, IL, USA). GLP-2 secretion was calculated using the following eq 4[23]

$$\text{GLP-2 secretion} = \frac{\text{extracellular GLP-2}}{\text{extracellular GLP-2} + \text{intracellular GLP-2}} \quad (4)$$

2.2.5.6. In Vitro qPCR Efficacy of LNC(H-151). J774 macrophages (2×10^5 cells/well) were placed in 24-well plates for 24 h. The cells were then treated with 0.5 or 0.05 μM H-151 or LNC(H-151). After 1 h, the cells were exposed to cGAMP (1.5 μg/mL) for stimulation. Nonstimulated untreated cells (CTRL) were used as a negative control and cGAMP-stimulated cells were used as a positive control (cGAMP). After 5 h of incubation, the supernatant was removed, and the mRNA of the cells was extracted and further processed by RT-qPCR.

Primary intraperitoneal macrophages (1×10^6 cells/well) were seeded in 24-well plates for 3 h at 37 °C in 5% CO_2. After being washed three times with PBS, the cells were seeded with medium. The cells were incubated with different formulations: H-151 0.5 μM or Blank LNC or H-151 0.5 μM + Blank LNC or LNC(H-151) 0.5 μM. After 1 h, the cells were exposed to cGAMP (1.5 μg/mL) for stimulation. Nonstimulated untreated cells (CTRL) were used as a negative control and cGAMP-stimulated cells were used as a positive control (cGAMP). After 5 h, the supernatant was removed, and the mRNA of the cells was extracted and further processed by RT-qPCR.

2.2.5.7. Western Blot Analysis. J774 macrophages (10^6 cells/well) were seeded onto 12-well plates for 24 h. The cells were then incubated with different formulations: H-151 0.5 μM or Blank LNC or H-151 0.5 μM + Blank LNC or LNC(H-151) 0.5 μM. After 1 h, the cells were exposed to cGAMP (1.5 μg/mL) for 3 h. Nonstimulated untreated cells (CTRL) were used as a negative control and cGAMP-stimulated cells were used as a positive control (cGAMP). The cells were lysed in 200 μL of lysis buffer (composition in Table S4). The cell lysates were diluted with 1:5 v/v loading dye [Lane marker Reducing sample buffer (5×)] and incubated for 10 min at 95 °C. Then, ∼8 μg of protein was loaded into each well of 4−15% gradient 15-well acrylamide gels. Afterward, 4 μL of Page Ruler Plus retained protein ladder (10−250 kDa) was loaded into the wells. The samples were subjected to electrophoresis (200 V, 1 h) using TRIS/Glycine/SDS buffer, transferred onto PVDF membranes using TRIS/Glycine buffer, blocked for 1 h in 5% (w/v) milk in TBS (1×)-Tween 20 0.1% (TBST), and then incubated overnight at 4 °C in primary antibody solutions (antibodies diluted in TBST with 5% (w/v) BSA [except 5% (w/v) milk for Histone 3H and pSTING)]. The membranes were washed 3 × 5 min in TBST and incubated for 1 h in secondary antibody solution (HRP-coupled mouse antirabbit IgG, diluted 1/10,000 in 5% (w/v) milk in TBST), washed 3 × 5 min in TBST, incubated for 1 × 5 min in TBS (1×), and visualized via SuperSignal West Pico PLUS or SuperSignal West Femto. The blot membranes were visualized using an Amersham ImageQuant800 from Cytiva (Marlborough, MA, USA), and the signals were quantified using ImageJ (National Institute of Health, Bethesda, MD, USA).[24] The antibodies and relative dilutions used here are reported in Table S5.

2.2.6. In Vivo Study. Animal experiments were performed in accordance with Belgian national regulation guidelines and were conducted in agreement with EU Directive 1010/63/EU concerning the use of animals for experimental purposes. The protocols were approved by the ethical committee for animal care of the UCLouvain (2023/UCL/MD/22). Male C57BL/6J mice (6 weeks old, 20−25 g) were purchased from Janvier Lab (Le Genest-St- Isle, France). The mice had access to water and food *ad libitum*, and their body weights were monitored every day during the experiment.

2.2.6.1. LNC(H-151) Efficacy in a Murine DSS-Induced Acute Colitis Model. The mice were randomly divided by weight into seven groups (8 mice/group): CTRL healthy, CTRL DSS, intraperitoneal (IP)-free H-151+ DSS, oral (OR)-free H-151+ DSS, OR Blank LNC + DSS, OR Blank LNC + free H-151 + DSS and OR LNC(H-151) + DSS. Colitis was induced through the administration of DSS (3% w/v) in the drinking water for 5 consecutive days. On days 4, 5, and 6, the mice were treated with 100−150 μL of the formulations (H-151 dose of 10.4 mg/kg via IP injection or 24 mg/kg OR). The CTRL healthy and CTRL DSS groups were administered orally with sterile PBS. Free H-151 was dissolved in a solution of 10% (v/v) Tween 80 in sterile PBS. Colonic inflammation was assessed on day 7. On the last day of the experiment, the mice were anesthetized with isoflurane, and colonoscopy videos were recorded to evaluate the severity of the disease macroscopically. Blood was collected from the portal and cava veins, and colon samples were collected to evaluate the severity of the colitis.

2.2.6.2. High-Resolution Colonoscopy. *In vivo* mouse colonoscopy was performed with a Coloview colonoscopy system from Karl Storz (Tuttlingen, Germany). On the last day of the study, the mice were anesthetized (with isoflurane), a mini endoscope was inserted through the anus, and the colon was insufflated with an air pump. Videos were recorded for

https://doi.org/10.1021/acs.molpharmaceut.4c01297
Mol. Pharmaceutics 2025, 22, 2108−2121

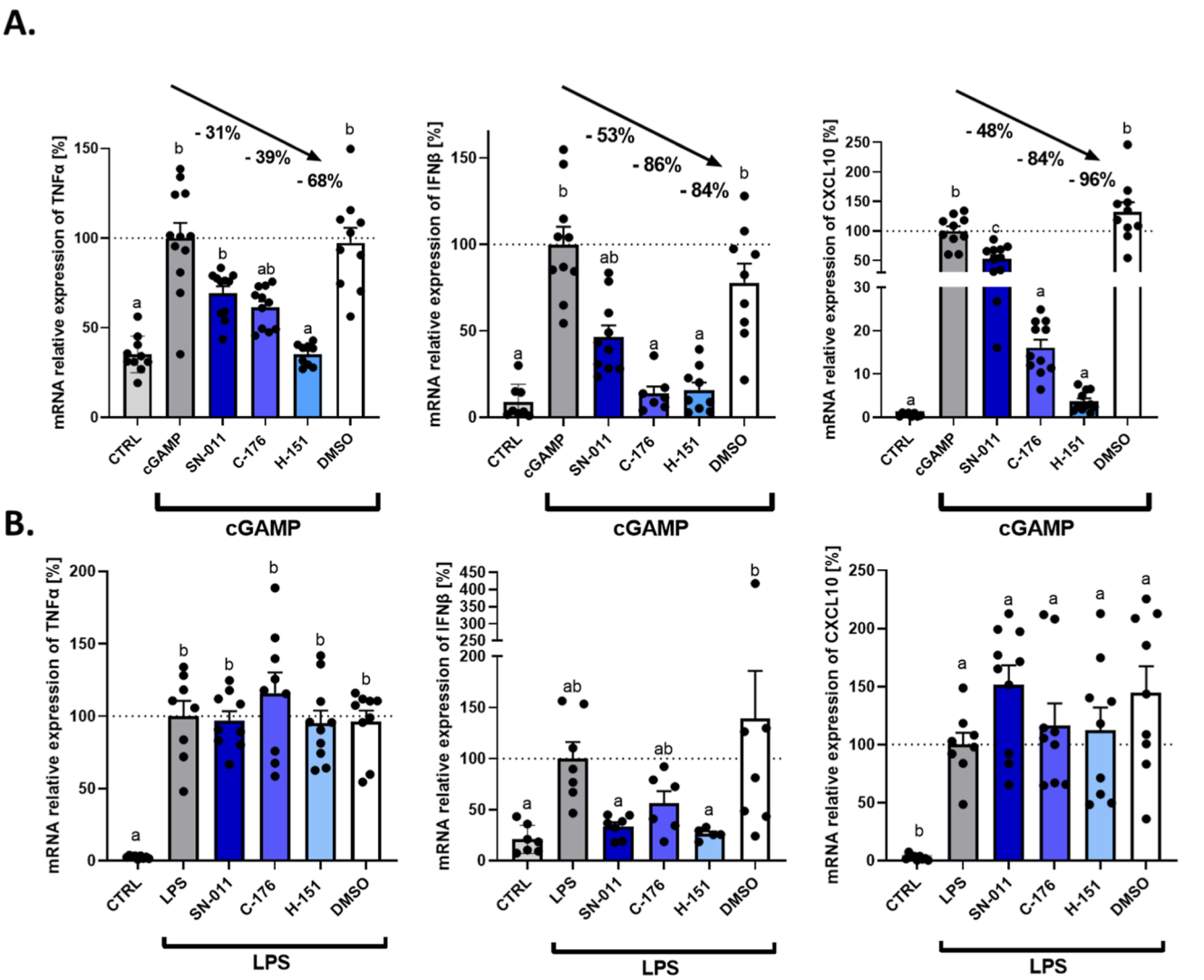

Figure 1. *In vitro* screening of cGAS-STING inhibitors in cGAMP- and LPS-activated J774 cells. A. Gene expression of cGAS-STING downstream markers associated with IBD after cGAMP or B. LPS activation in J774 cells. The cells were treated with 0.5 μM SN-011, C-176, or H-151. DMSO in medium was used as vehicle control, cGAMP-activated (cGAMP) or LPS-activated (LPS) cells were used as positive controls, and CTRL was used as a negative control (nonactivated with cGAMP or LPS). The data were normalized to those of the cGAMP or LPS group. The arrows represent the relative reduction in the inhibitor groups compared with the cGAMP groups. Data with different superscript letters were considered significantly different ($^*p < 0.05$) according to one-way ANOVA followed by Tukey's post hoc test (A: CXCL10; B: TNF-α, IFN-β, and CXCL10) or the Kruskal–Wallis test followed by Dunn's posthoc test (A: TNF-α, IFN-β) (mean ± SEM; $N = 3$, $n = 4$).

each mouse, and images were captured from the videos. The colitis score (murine endoscopic index of colitis severity, MEICS) was scored as described by Becker et al.[25] focusing on five parameters: the thickening of the colon, changes in the vascular pattern, visible fibrin, granularity of the mucosal surface, and stool consistency. Each parameter was graded between 0 and 3 depending on the severity of the disease.[25] Colonoscopy scoring was performed in a double-blinded manner.

2.2.6.3. Colon Weight/Length Ratio. After the mice were sacrificed, their colons were harvested, and any fecal matter was removed with DPBS. The colonic tissues were then weighed. The lengths were measured from the beginning of the proximal part to the anus using a digital caliper gauge (0−150 mm) from Carl Roth GmbH (Karlsruhe, Germany). The weight/length ratio of the colons was then calculated.

2.2.6.4. Myeloperoxidase (MPO) Activity. Colonic tissues were homogenized twice with 500 μL of HTAB buffer (0.5% HTAB in 50 mM KH_2PO_4 buffer, pH = 6) (40% amplitude, 10 s with a Branson 450 Digital Sonifier from Branson Ultrasonics, Brookfield, CT, USA) while kept on ice. The homogenates were subsequently centrifuged at 20,000*g* for 10 min at 4 °C. Next, 7 μL of the supernatant was added to 200 μL of the MPO analysis solution (50 mM KH_2PO_4 buffer pH = 6 containing 0.147 mg/mL *o*-dianisidine and 500 ppm of H_2O_2) in a 96-well plate. The MPO activity was measured with a spectrophotometer (SpectraMax iD5, Molecular Devices, San Jose, CA, USA) at 460 nm every minute for 30 min. The results were normalized to the protein content, which was quantified with a Pierce BCA protein assay kit (Sigma-Aldrich, St. Louis, MO, USA). The results are expressed as MPO units per milligram of tissue, considering that one unit of MPO activity was expressed as the amount that degrades 1 mmol/min of H_2O_2 at 25 °C.[26,27]

2.2.6.5. Histological Scoring. Histological scores were determined in a double-blinded manner by three different

https://doi.org/10.1021/acs.molpharmaceut.4c01297
Mol. Pharmaceutics 2025, 22, 2108−2121

A.

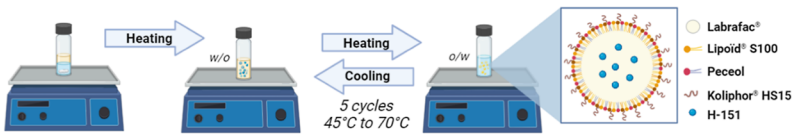

B.

Formulation	Size [nm]	PdI	ζ Potential [mV]	EE [% w/w]	DL [% w/w]
Blank LNC	177.08 ± 1.21	0.065 ± 0.02	-6.99 ± 1.19	-	-
LNC(H-151)	167.68 ± 1.45	0.091 ± 0.01	-9.26 ± 0.70	99.95	1.57

Figure 2. Preparation and characterization of LNC(H-151). (A) Schematic representation of the phase inversion procedure used to prepare LNC(H-151). (B) Physicochemical characterization of the formulation, including size, PdI, zeta potential, H-151 encapsulation efficiency (EE, % w/w), and drug loading (DL, % w/w).

researchers and are expressed as the means of the three analyses as described by Koelink et al.[28] Small segments of the colon were fixed in ROTI Histofix 4% formaldehyde solution (pH = 7), washed with 70% ethanol, and subsequently embedded in paraffin. Two sets of three serial sections were cut 150 μm apart, resulting in two slide analyses per mouse. The sections were stained with hematoxylin−eosin (H&E). The histological scoring items included the presence of inflammatory infiltrate, goblet cell loss, crypt density, crypt hyperplasia, muscle thickening, submucosal inflammation, crypt abscess, and ulceration, with each parameter being graded between 0 and 3.

2.2.6.6. Cytokine and Chemokine Quantification by ELISA. Colon homogenates were directly prepared from tissue samples frozen at −80 °C in ice-cold lysis buffer (ultrapure water with 500 nM NaCl, 2 mM EDTA, 1% Triton X-100, 0.5% sodium deoxycholic acid, 0.1% SDS, 50 mM Tris−HCl and 1 tablet of protease inhibitor cocktail per 10 mL of solution). The colon tissues were weighed, and a volume of lysis buffer was added to achieve a normalized concentration of 15 mg of tissue/100 μL of lysis buffer. The samples were homogenized twice by sonication (Branson 450 digital sonifier, 40% amplitude, 10 s) and centrifuged (20,000*g* for 10 min). The supernatant was retrieved and stored at −80 °C until further analysis. The concentrations of colonic pro-inflammatory cytokines and chemokines were determined with a V-PLEX Custom Mouse Biomarkers with Proinflammatory Panel 1 and Cytokine Panel 1 purchased from Meso Scale Diagnostics (Rockville, MD, USA). The plates were used in accordance with the manufacturer's instructions and read using a MESO QuickPlex SQ 120 plate reader from Meso Scale Diagnostics (Rockville, MD, USA). The quantified pro-inflammatory cytokines and chemokines were IFN-γ, IL-1β, IL-6, KC/GRO, IL-12p70, IL-17AF, CXCL10, MCP-1, MIP-1α, and TNF-α. The protein concentrations were normalized to the protein content and quantified with a Pierce BCA protein assay kit (Sigma-Aldrich, St. Louis, MO, USA). The results are expressed relative to those of the CTRL DSS group.

2.2.7. Statistical Analysis. Statistical analysis was conducted using the *GraphPad Prism 10* program (La Jolla, CA, USA). A Grubbs outlier test was performed in every group to support any exclusion. A Shapiro−Wilk test was performed to investigate the normality of the distribution in the groups. Statistical analyses of multiple groups were conducted using one-way analysis of variance (ANOVA) followed by Tukey's multiple comparison post hoc test (parametric) and the Kruskal−Wallis test followed by Dunn's multiple comparison post hoc test (nonparametric). A *t*-test (parametric) or Mann−Whitney test (nonparametric) was performed for comparisons between two groups. The results are expressed as the means ± standard error of the means (SEM). A p value <0.05 was considered statistically significant. *p < 0.05, **p < 0.01, ***p < 0.001 and ****p < 0.0001.

3. RESULTS AND DISCUSSION

3.1. H-151 Displayed an Increased Efficacy for cGAS-STING Pathway Inhibition in J774 Macrophages. We performed an *in vitro* screening of three cGAS-STING inhibitors, namely, SN-011, C-176, and H-151, by assessing their efficacy at inhibiting the cGAS-STING pathway in murine macrophage J774 cells (Figure 1).[29] SN-011 is a potent and selective mouse and human STING inhibitor. Compared with endogenous cGAMP, SN-011 binds with greater affinity to the CDN-binding pocket of STING, making STING form an open, inactive conformation.[30] However, C-176 (mouse-specific) and H-151 (mouse- and human-specific) are highly potent inhibitors that covalently bind with cysteine 91 (Cys91) of STING, preventing the palmitoylation required for STING activation and downstream signaling.[11,31] Macrophages were selected because they are the most representative cells of innate immunity and are therefore of great interest in the context of cGAS-STING investigations.[32] All the inhibitors displayed a comparable molecular weight associated with a Log P > 3 and low water solubility but were slightly soluble in ethanol or DMSO (Figure S1). The pK_a values were found to be 6.6, 12.62, and 11.48 for SN-011, C-176, and H-151, respectively.[33]

The expression of TNF-α (a key player in IBD inflammation), IFN-β (a type 1 interferon that plays a key role in autoimmune and inflammatory diseases and is mediated by the cGAS-STING pathway), and CXCL10 (a downstream marker of cGAS-STING complex activation) were used as readouts of the efficacy of cGAS-STING inhibition.[34−36] As shown in Figure 1A, all the studied compounds were able to decrease the expression of the selected markers when activated with cGAMP, whereas the impact of the vehicle (DMSO) was negligible. SN-011 and C-176 decreased the expression of TNF-α (31% and 39%, respectively, with respect to the cGAMP group), although the differences were not significant. However, H-151 significantly reduced the expression of TNF-α (68%, ****p < 0.0001) compared with that in the cGAMP group. Compared with that in the cGAMP group, IFN-β expression was significantly lower in the C-176 (86%, **p < 0.01) and H-151 (84%, ***p < 0.001) groups but not in the

https://doi.org/10.1021/acs.molpharmaceut.4c01297
Mol. Pharmaceutics 2025, 22, 2108−2121

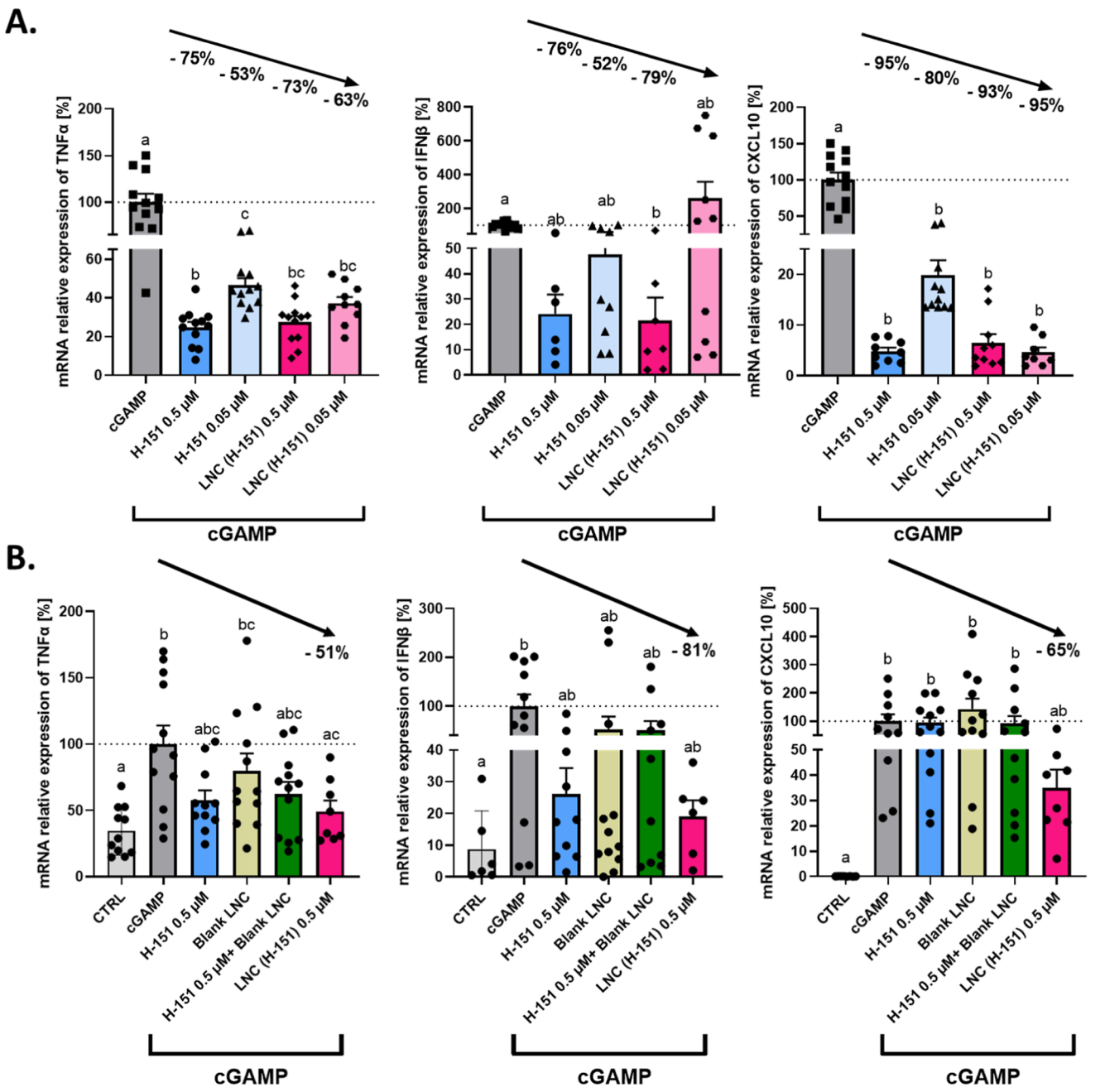

Figure 3. LNC(H-151) inhibits the cGAS-STING pathway *in vitro* in J774 and primary IP macrophages. (A) Gene expression of cGAS-STING downstream markers associated with pro-inflammatory markers in IBD after cGAMP activation of J774. The cells were treated with H-151 or LNC(H-151) at 0.5 or 0.05 μM. or (B). Gene expression of cGAS-STING downstream markers associated with pro-inflammatory markers in IBD after cGAMP activation of primary IP macrophages. Primary IP macrophages extracted from C57BL/6J mice were treated with H-151 0.5 μM, Blank LNC, H-151 0.5 μM + Blank LNC or LNC(H-151). Nonstimulated untreated cells (CTRL) were used as a negative control and cGAMP-stimulated cells were used as a positive control (cGAMP). The data were normalized to those of the cGAMP group. The arrows represent the relative reduction between the cGAMP group and the treatment groups. Data with different superscript letters were considered significantly different (*$p < 0.05$) according to one-way ANOVA followed by Tukey's post hoc test (A: TNF-α and CXCL10; B: TNF-α) or the Kruskal–Wallis test followed by Dunn's post hoc test (A: IFN-β; B: IFN-β and CXCL10) (mean ± SEM; $N = 3$, $n = 4$).

SN-011 group, even though the reduction was 53% compared with that in the cGAMP group.

All the inhibitors also significantly reduced the expression of CXCL10 in SN-011, C-176, and H-151, with reductions of 48% (***$p < 0{,}001$), 84% (****$p < 0{,}0001$), and 96% (****$p < 0{,}0001$), respectively, compared with those in the cGAMP group. Taken together, these data suggest the superior efficacy of H-151 at inhibiting the cGAS-STING pathway; thus, H-151 was selected for subsequent studies.

The selectivity of these inhibitors for the cGAS-STING pathway was also studied by evaluating their effects on J774 macrophages activated with LPS (Figure 1B). We did not observe differences in any of the cytokines investigated when comparing all the LPS-treated groups together, confirming the specificity of the inhibitors for the cGAS-STING pathway.

https://doi.org/10.1021/acs.molpharmaceut.4c01297
Mol. Pharmaceutics 2025, 22, 2108−2121

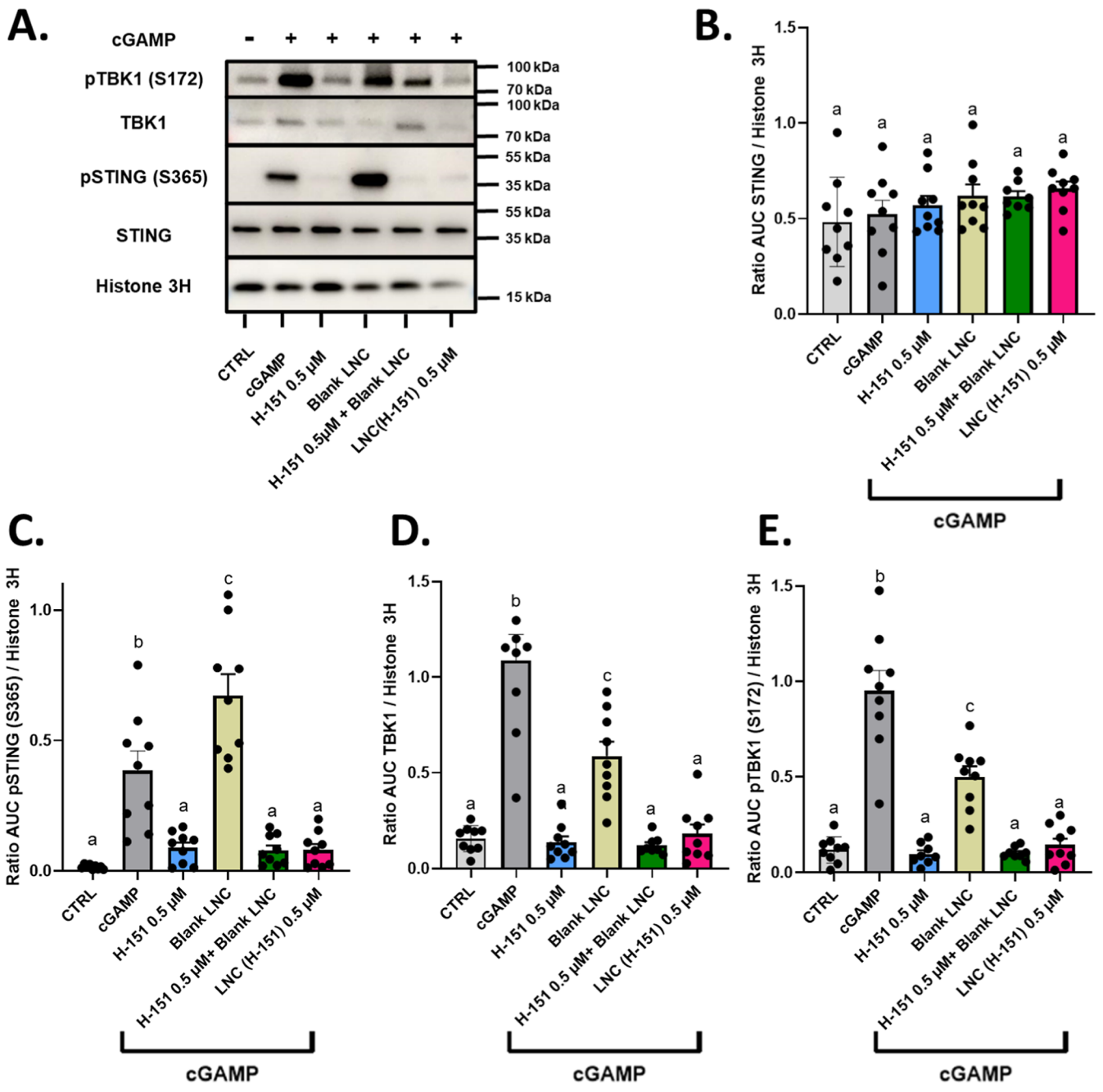

Figure 4. LNC(H-151) reduces TBK1 expression and the phosphorylation of STING and TBK1 *in vitro* in J774 cells. (A) Expression of proteins involved in the cGAS-STING pathway after cGAMP activation in J774. The cells were treated with H-151 0.5 μM, Blank LNC, H-151 0.5 μM + Blank LNC, LNC(H-151) 0.5 μM for 1 h. Then, cGAMP was added for 3 h. Nonstimulated untreated cells (CTRL) were used as a negative control and cGAMP-stimulated cells were used as a positive control (cGAMP). The cells were lysed and analyzed by Western blotting with anti-Histone 3H (as a loading control), anti-STING, anti-p-STING (S365), anti-TBK1, and anti-pTBK1 antibodies. Representative blots are presented in order. (B) Quantification of the STING protein, (C) pSTING, (D) TBK1 and (E) pTBK1 after cGAMP activation in J774 cells. Blot signals were quantified using ImageJ, and every signal was normalized to its associated Histone 3H signal to normalize to the corresponding amount of protein. Data with different superscript letters were considered significantly different (*$p < 0.05$) according to one-way ANOVA followed by Tukey's post hoc test (mean ± SEM; $N = 3$, $n = 3$).

Since bacterial LPS also plays a key role in the inflammatory process of IBD,[37] these results suggest that a combinatorial strategy for modulating both LPS-induced and cGAS-STING-induced inflammation could be interesting for effectively treating IBD.

3.2. Preparation and Characterization of LNC(H-151).

LNCs were selected based on their ability to encapsulate poorly water-soluble drugs, improve drug solubility and protect drugs from degradation in the GI tract.[38−40] LNCs also induce GLP-2 secretion, which is known to be associated with crypt cell proliferation, inhibition of apoptosis in enterocytes, and promoting re-epithelization.[1,23,41,42] LNCs loaded with H-151 [referred to as LNC(H-151)] were prepared using the phase reversion process (Figure 2A). The EE was 99.95% and the DL was 1.57%. Pilot studies were performed with lower and higher amounts of drug; however, these batches resulted unsat-

https://doi.org/10.1021/acs.molpharmaceut.4c01297
Mol. Pharmaceutics 2025, 22, 2108−2121

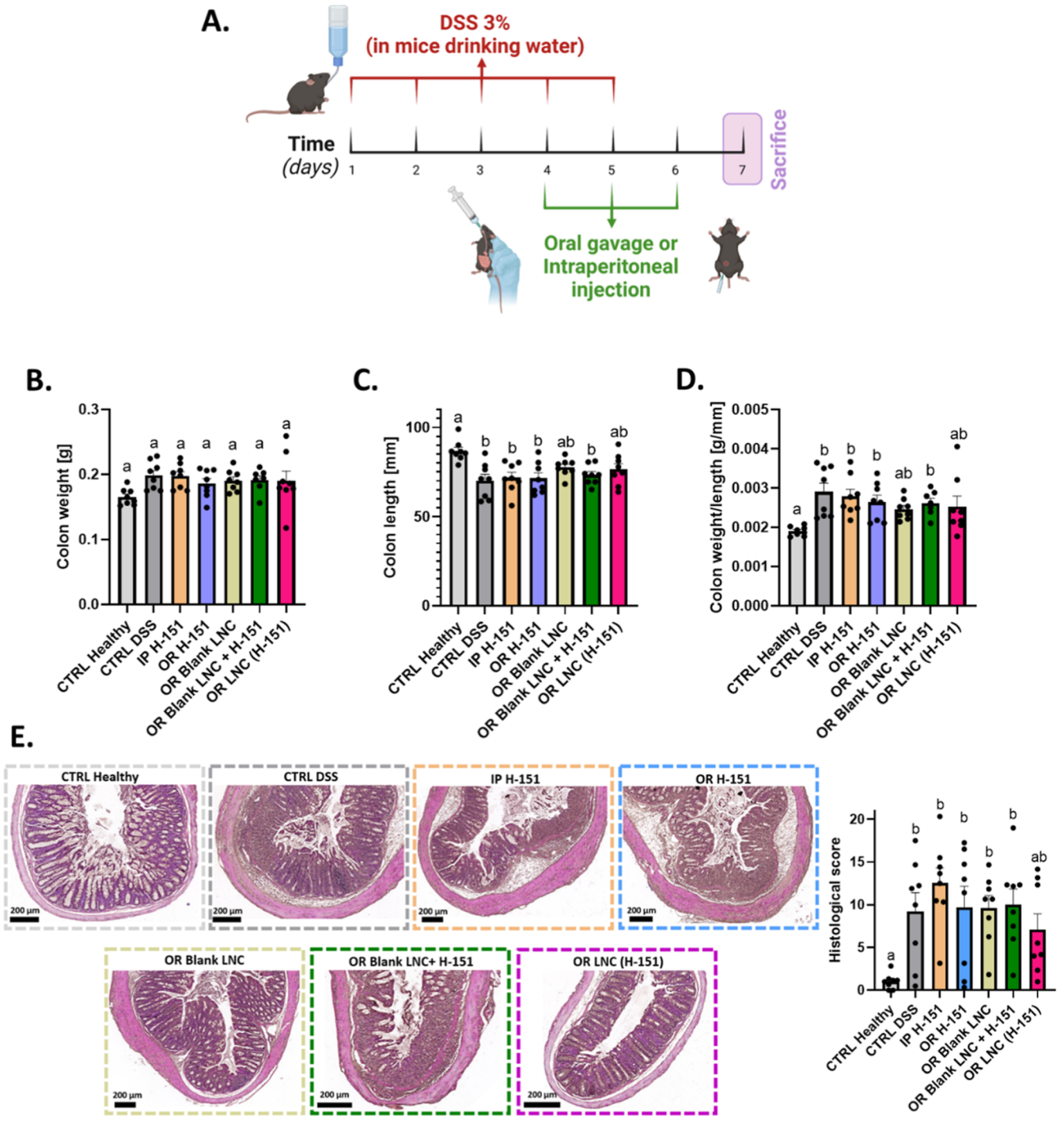

Figure 5. Oral treatment with LNC(H-151) exerted an anti-inflammatory effect in a DSS-induced acute colitis model. (A) Scheme illustrating the induction of colitis. (B) Colon weight (g) (n = 7−8). (C) Colon length (mm) (n = 7−8). (D) Colon weight/length ratio (g/mm) (n = 7−8). (E) Histological images (H&E-stained images with a scale bar of 200 μm) and results of double-blinded histological scoring (n = 16). Colonic tissues were harvested after the mice were sacrificed on day 7. Data with different superscript letters are significantly different (*p < 0.05) according to one-way ANOVA followed by Tukey's post hoc test (B,C,E.) or the Kruskal−Wallis test followed by Dunn's post hoc test (D). (mean ± SEM). DSS: Dextran sodium sulfate; CTRL: control; IP: intraperitoneal; OR: oral administration; Blank LNC: unloaded lipid nanocapsules; and LNC(H-151): lipid nanocapsules encapsulating H-151.

isfactory in terms of drug loading, or were leading to drug precipitation. The size of the Blank LNC was 177.08 ± 1.21 nm, while LNC(H-151) was 167.68 ± 1.45 nm. The PdI values were 0.065 ± 0.02 and 0.091 ± 0.01, respectively. The zeta potentials were negative: −6.99 ± 1.19 mV and −9.26 ± 0.70 mV, respectively. Furthermore, LNC(H-151) was stable over time in terms of size and PdI when maintained at 4 °C (Figure S2). Additionally, a cell viability study of LNC(H-151) in J774 cells revealed no toxicity (above 80% viability) at doses up to 1 μM (Figure S3). We confirmed that, compared with the CTRL, LNC(H-151) preserved the ability to secrete GLP-2 upon encapsulation of H-151 in the GLUTag murine L cell line (Figure S4). We also investigated the drug release in simulated GI fluids (Figure S5A). Almost no cumulative drug

https://doi.org/10.1021/acs.molpharmaceut.4c01297
Mol. Pharmaceutics 2025, 22, 2108−2121

release from the LNC(H-151) could be observed in FASSGF (0.79% after 2 h) and FASSIF (0.29% after 3 h). In FASSCOF, after 12 h, 9.10% of the drug was released from the LNC(H-151) and it reached 13.68% after 24 h. Those results are in agreement with other studies with lipophilic drugs encapsulated in LNCs.[19,20] The stability of the size, PdI, and concentration of LNC(H-151) were also investigated in FASSGF, FASSIF, FASSCOF (Figure S5B,C). In all of the simulated GI fluids, the size and PdI were stable over the 6 h. Concerning the concentration of LNC(H-151), we observed a decrease in nanoparticle concentration over 6 h in FASSGF (22%) but they remained stable in the FASSIF and FASSCOF.

3.3. LNC(H-151) Efficiently Inhibits the cGAS-STING Pathway in J774 and IP Macrophages. Several studies suggest that lipid-based nanoparticles can improve the cellular uptake, internalization, and release of cargo drugs in the cytosol.[43−45] We hypothesized that the encapsulation of the inhibitor within LNCs could improve the efficacy of cGAS-STING inhibitors by facilitating their intracellular delivery. To investigate this phenomenon, we explored whether LNC(H-151) could better inhibit cGAS-STING and evaluated the expression of associated cytokines compared to free H-151 in J774 macrophages (Figure 3A). Both free H-151 and LNC(H-151) inhibited TNF-α and CXCL10 in J774 macrophages. Compared with the cGAMP group, all the groups presented a reduction in TNF-α expression (75% for H-151 0.5 μM, ****$p < 0.0001$; 53% for H-151 0.05 μM, ****$p < 0.0001$; 73% for LNC(H-151) 0.5 μM, ****$p < 0.0001$; 63% for LNC(H-151) 0.05 μM, ****$p < 0.0001$). Compared with H-151 0.5 μM, LNC(H-151) 0.05 μM resulted in a comparable reduction in TNF-α levels, confirming the efficacy of the encapsulated inhibitor compared with the free inhibitor, even at a 10-fold lower dose. Additionally, LNC(H-151) 0.5 μM was the only group to significantly reduce the expression of IFN-β (79%, **$p < 0.01$) compared to the cGAMP group. The reduction in CXCL10 expression was significant for both the free inhibitor groups (95% for H-151 0.5 μM, ****$p < 0.0001$ and 80% for H-151 0.05 μM, ****$p < 0.0001$) and both the encapsulated inhibitor groups (93% for LNC(H-151) 0.5 μM, ****$p < 0.0001$ and 95% for LNC(H-151) 0.05 μM, ****$p < 0.0001$). Although they were not significantly different, we observed a notable trend toward a reduction in CXCL10 expression in LNC(H-151) cells at 0.05 μM, with a 4-fold reduction compared with that in free H-151 at a similar concentration.

The efficacy of LNC(H-151) was also studied in primary IP macrophages (Figure 3B). Primary cells were investigated due to their greater biological relevance compared to immortalized cell lines, as well as their higher heterogeneity, original genome and preserved phenotypic characteristics.[46] Additionally, macrophages drive the activation of the cGAS-STING pathway, which is particularly important in IBD.[14,32] Compared with the cGAMP group, LNC(H-151) was the only group that significantly reduced TNF-α expression (51%, *$p < 0.05$). Compared with those in the cGAMP and CTRL groups, the levels of IFN-β in all the treatment groups were similar and did not differ. Nevertheless, LNC(H-151) still resulted in a reduction in IFN-β expression (81%) compared to the cGAMP group. LNC(H-151) also reduced the expression of CXCL10 compared to the cGAMP group (65%), but this difference was not significant. Compared with the CTRL group, the LNC(H-151) group was also the only group with a similar level of expression.

Overall, these results confirm the hypothesis that LNCs encapsulation can improve the efficacy of H-151 inhibitors and help decrease the expression of pro-inflammatory cytokines associated with the cGAS-STING pathway.

3.4. LNC(H-151) Reduces TBK1 Expression and the Phosphorylation of TBK1 and STING in J774 Macrophages. Based on the previous *in vitro* results, we further evaluated whether LNC(H-151) was able to directly inhibit the expression and phosphorylation of STING and related downstream markers (e.g., TBK1) (Figures 4 and S6).[12,32,47] We observed no effect of the treatments on STING expression (Figure 4B). This result was expected since H-151 exerts its inhibitory effect by covalently binding to STING at the transmembrane cysteine residue at position 91, blocking its palmitoylation and further activation.[11,31] Notably, we observed reduced expression of downstream markers of STING activation, including pSTING (S365), TBK1, and pTBK1 (S172) (cGAMP vs LNC(H-151) 0.5 μM, ***$p <$ 0.001) (Figure 4C−E). Although no differences in efficacy were observed between H-151 0.5 μM, H-151 0.5 μM + Blank LNC, and LNC(H-151) 0.5 μM, our findings showed that the encapsulation does not alter the pharmacodynamic properties of the drug, retaining its ability to inhibit the targeted pathway. Interestingly, we observed that Blank LNC increased the expression of pSTING (**$p < 0.01$) and reduced the expression of TBK1 (****$p < 0.0001$) and pTBK1 (****$p < 0.0001$). It would be interesting to further study how Blank LNC affect the cGAS-STING pathway.

3.5. Effect of LNC(H-151) in a Murine DSS-Induced Acute Colitis Model. To investigate the efficacy of our formulation in IBD treatment, we evaluated the effect of LNC(H-151) in a murine DSS-induced acute colitis model (Figure 5A). This model is one of the most widely used mouse models of colitis and is independent of T cells and in favor of innate immune cells (such as macrophages and neutrophils), thus representing a valuable model for investigating the role of the innate immune system in the context of intestinal inflammation.[48] Given that the cGAS-STING pathway plays a crucial role in initiating the innate immune response,[10] we opted to test our formulation in a murine DSS-induced acute colitis model.

To recapitulate the clinical conditions of patients affected by IBD, treatments were started on day 4 when the symptoms of the disease started, and the formulations were administered for 3 consecutive days (days 4−6).[49] Mice treated with IP injections (H-151 dose of 10.4 mg/kg as reported in previous in vivo studies) were used as controls.[11,31,50−52] An oral dose of 24 mg/kg H-151 was considered based on the volume of administration per gavage and the maximum concentration of encapsulated H-151. No significant changes in body weights were observed among the DSS-treated groups within the study (Figure S7).

Since colitis is known to induce colon shortening and increase the density of colonic tissue,[48] the weights and lengths of the colons were measured at the end point of the experiment (Figure 5B−C). The colon length results revealed a decrease in the sizes of all the groups compared with that of the CTRL Healthy group, except for the OR Blank LNC and OR LNC(H-151). Similar results were observed when the colon weight/length ratio was analyzed (CTRL Healthy vs IP H-151, **$p < 0.01$; CTRL Healthy vs OR H-151, *$p < 0.05$; and CTRL Healthy vs OR Blank LNC + H-151, *$p < 0.05$) (Figure 5D). These results suggest that the Blank LNC have an

https://doi.org/10.1021/acs.molpharmaceut.4c01297
Mol. Pharmaceutics 2025, 22, 2108−2121

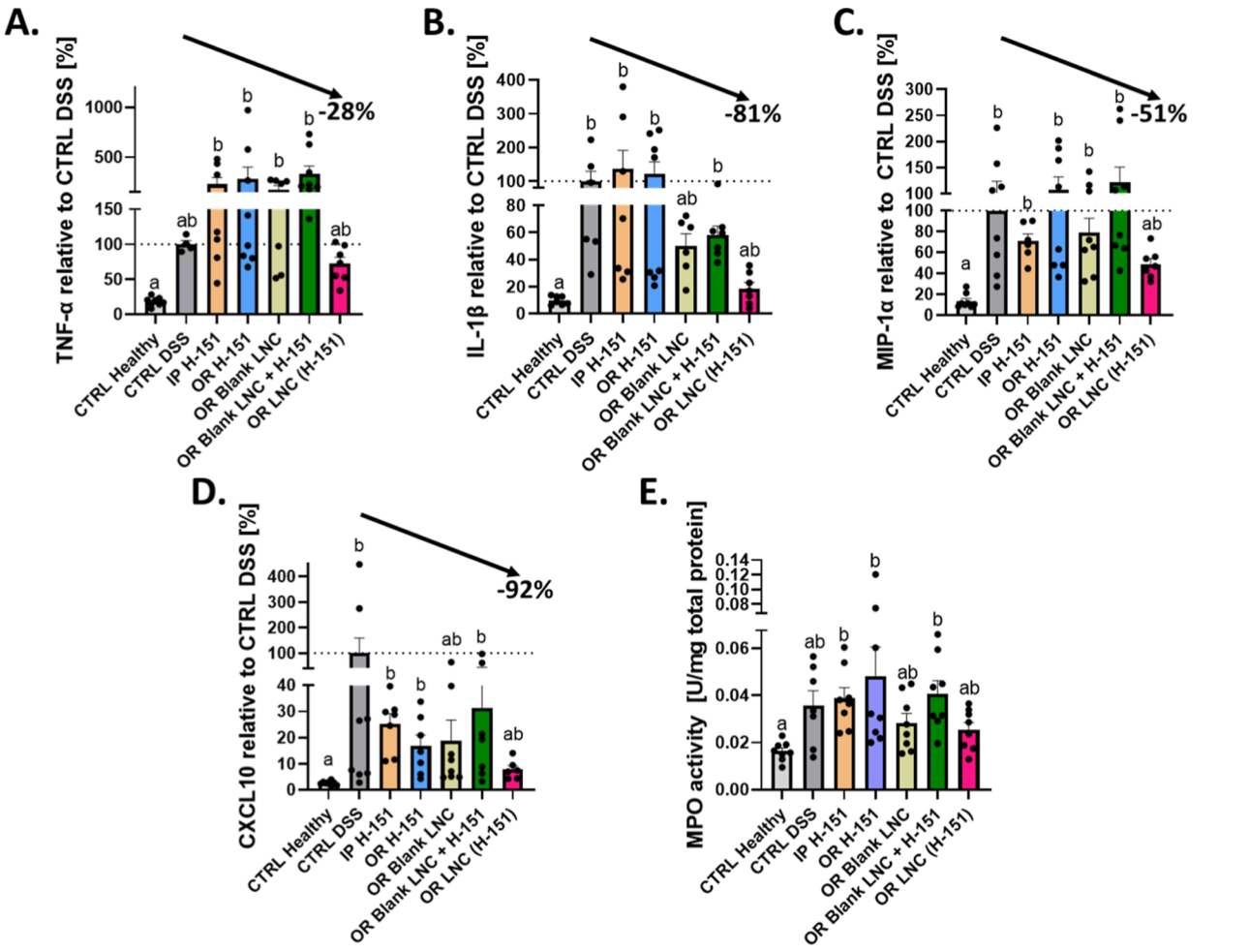

Figure 6. Pro-inflammatory cytokine/chemokine expression and MPO activity in the colon following treatment in a DSS-induced acute colitis model. (A) TNF-α expression (n = 4−8). (B) IL-1β expression (n = 6−8). (C) MIP-1α expression (n = 6−8). (D) CXCL10 expression (n = 6−8). E. MPO activity in the colon at 8 min (U/mg total protein) (n = 8). The data in A, B, C, and D are presented as normalized to the CTRL DSS. The arrows represent the relative reduction between the CTRL DSS (positive control) and OR LNC(H-151) groups. Data with different superscript letters are significantly different (*p < 0.05) according to the Kruskal−Wallis test followed by Dunn's post hoc test (mean ± SEM). DSS: Dextran sodium sulfate; CTRL: control; IP: intraperitoneal; OR: oral administration; Blank LNC: unloaded lipid nanocapsules; and LNC(H-151): lipid nanocapsules encapsulating H-151.

effect per se, most likely induced by the GLP-2 re-epithelizing effect.

The blinded histological scoring analysis performed on the colon sections (Figure 5E) revealed that OR LNC(H-151) had a comparable histological score to that of the CRTL Healthy group but was not different from that of the CTRL DSS group. This effect is illustrated in Figure 5E, which compares histological sections and reveals differences, especially in terms of muscle thickening and submucosal inflammation. However, all the DSS-treated groups were comparable. Considering colonoscopy evaluation, no differences among the groups were observed (Figure S8).

Macro/microscopic observations revealed that OR LNC(H-151) treatment resulted in comparable parameters to those of the CTRL Healthy group (e.g., colon length, colon weight/length ratio, histological score), indicating better efficacy at attenuating the immune response in a DSS-induced acute colitis model, although the formulation was only administered for three consecutive days.

Next, we studied the effects of the formulations on the release of pro-inflammatory markers in colon tissues and their effects on the recruitment of neutrophils as innate immune mucosal modulators (Figure 6A−D and S10). OR LNC(H-151) showed remarkable efficacy at reducing TNF-α, IL-1β, MIP-1α, and CXCL10 expression to levels comparable to those in the CTRL Healthy group. In particular, the OR LNC(H-151) displayed 3.17-fold, 2.46-fold and 4.64-fold reductions in TNF-α compared with those of IP H-151, OR Blank LNC, and OR Blank LNC + H-151 respectively, even though this effect was not significant. Similar trends were found for IL-1β, MIP-1α, and CXCL10. Thus, the encapsulated inhibitor was more efficient at reducing inflammatory cytokines/chemokines than the empty LNCs mixed with the free drug. Overall, these findings confirm the efficacy of OR LNC(H-151) at restoring inflammatory cytokine and chemokine levels in the colon to those observed in healthy controls via cGAS-STING inhibition. Furthermore, these results emphasize the superior effectiveness of the encapsulated inhibitor compared with the inhibitor alone in vivo, as neither IP H-151, OR H-151, nor OR Blank LNC + H-151 were able to restore healthy levels of any of those four inflammatory markers.

Considering the reduction in cytokine levels, we hypothesized that OR LNC(H-151) treatment could also modulate

https://doi.org/10.1021/acs.molpharmaceut.4c01297
Mol. Pharmaceutics 2025, 22, 2108−2121

mucosal innate immunity. Therefore, we assessed MPO in colon lysates to evaluate neutrophil infiltration, a biomarker of inflammation in IBD patients (Figure 6E).[53−56] We observed that the levels of IP H-151, OR H-151, and OR Blank LNC + H-151 were significantly greater than those of the CTRL Healthy group, whereas the levels of OR Blank LNC and OR LNC(H-151) were comparable to those of the CTRL healthy group. Additionally, looking at the full kinetic profile (Figure S9), the OR LNC(H-151) is the closest to the CTRL Healthy results. These data are consistent with the observed cyto-/chemokine profiles, suggesting that LNC(H-151) can inhibit the cGAS-STING pathway and prevent the infiltration of neutrophils that participate in the disruption of the crypt architecture of the intestine, promoting tissue damage.[9] However, additional studies are needed to confirm this hypothesis.

4. CONCLUSION

In this work, we described an oral formulation to deliver the cGAS-STING inhibitor H-151 in the context of IBD treatment. Our preliminary screening findings suggest that H-151 might be used to inhibit the cGAS-STING pathway and that the effects can be potentiated after encapsulation within LNCs. Our cost-effective and easily scalable formulation effectively ameliorated the inflammatory state by inhibiting the cGAS-STING pathway in both immortalized and primary macrophages. Our findings demonstrate that three daily oral administrations of our formulation effectively reduced inflammation markers to levels comparable to those of healthy controls within a murine DSS-induced acute colitis model. Moreover, our strategy reveals the possibility of combining our treatment with other approaches that target several arms of the IBD immune response, such as adaptative-induced inflammation. Future studies are warranted to optimize the colon-specific targeting of LNCs to increase their therapeutic efficacy in IBD treatment.

■ ASSOCIATED CONTENT

Supporting Information

The Supporting Information is available free of charge at https://pubs.acs.org/doi/10.1021/acs.molpharmaceut.4c01297.

Detailed LNC content formulation, composition of the GI biomimetic media, RT-qPCR primer sequences, composition of lysis buffer and antibodies information for Western blot, cGAS-STING inhibitors chemical structure and physicochemical characteristics, stability study of LNC, cell viability of H-151 and LNC(H-151), GLP-2 secretion study of LNC(H-151) on GLUTag cells, drug release and stability study of LNC(H-151) in GI media, all complete Western blot images, weight evolution/colonoscopy/MEICS score/MPO profile/cyto-chemokine expression of in vivo study (PDF)

■ AUTHOR INFORMATION

Corresponding Authors

Alessio Malfanti − *Department of Pharmaceutical and Pharmacological Sciences, University of Padova, 35131 Padova, Italy;* orcid.org/0000-0002-3694-8667; Phone: +32 (0)27647320; Email: ana.beloqui@uclouvain.be

Ana Beloqui − *Louvain Drug Research Institute, Advanced Drug Delivery and Biomaterials, UCLouvain, Université Catholique de Louvain, 1200 Brussels, Belgium; WEL Research Institute, 1300 Wavre, Belgium;* orcid.org/0000-0003-4221-3357; Phone: +39 0498275688; Email: alessio.malfanti@unipd.it

Authors

Léo Guilbaud − *Louvain Drug Research Institute, Advanced Drug Delivery and Biomaterials, UCLouvain, Université Catholique de Louvain, 1200 Brussels, Belgium;* orcid.org/0009-0007-3892-497X

Cheng Chen − *Louvain Drug Research Institute, Advanced Drug Delivery and Biomaterials, UCLouvain, Université Catholique de Louvain, 1200 Brussels, Belgium*

Inês Domingues − *Louvain Drug Research Institute, Advanced Drug Delivery and Biomaterials, UCLouvain, Université Catholique de Louvain, 1200 Brussels, Belgium*

Espoir K. Kavungere − *Louvain Drug Research Institute, Advanced Drug Delivery and Biomaterials, UCLouvain, Université Catholique de Louvain, 1200 Brussels, Belgium*

Valentina Marotti − *Louvain Drug Research Institute, Advanced Drug Delivery and Biomaterials, UCLouvain, Université Catholique de Louvain, 1200 Brussels, Belgium;* orcid.org/0000-0002-7273-0868

Hafsa Yagoubi − *Louvain Drug Research Institute, Advanced Drug Delivery and Biomaterials, UCLouvain, Université Catholique de Louvain, 1200 Brussels, Belgium*

Wunan Zhang − *Louvain Drug Research Institute, Advanced Drug Delivery and Biomaterials, UCLouvain, Université Catholique de Louvain, 1200 Brussels, Belgium*

Complete contact information is available at: https://pubs.acs.org/10.1021/acs.molpharmaceut.4c01297

Notes

The authors declare no competing financial interest.

■ ACKNOWLEDGMENTS

We thank Rose-Marie Goebbels for her assistance with histology staining. A.B. is a research associate from the Belgian FRS-FNRS (Fonds de la Recherche Scientifique) and a WEL Research Institute investigator (WELBIO-CR-2022 S−01). Images were created with GraphPad Prism 10 or Biorender.com.

■ REFERENCES

(1) Marotti, V.; Xu, Y.; Bohns Michalowski, C.; Zhang, W.; Domingues, I.; Ameraoui, H.; Moreels, T. G.; Baatsen, P.; Van Hul, M.; Muccioli, G. G.; Cani, P. D.; Alhouayek, M.; Malfanti, A.; Beloqui, A. A Nanoparticle Platform for Combined Mucosal Healing and Immunomodulation in Inflammatory Bowel Disease Treatment. *Bioact. Mater.* **2024**, *32*, 206−221.

(2) Zhang, W.; Michalowski, C. B.; Beloqui, A. Oral Delivery of Biologics in Inflammatory Bowel Disease Treatment. *Front Bioeng Biotechnol* **2021**, *9*, 675194.

(3) Zhang, W.; McCartney, F.; Xu, Y.; Bohns Michalowski, C.; Domingues, I.; Kambale, E. K.; Moreels, T. G.; Guilbaud, L.; Chen, C.; Marotti, V.; Brayden, D. J.; Beloqui, A. An in Situ Bioadhesive Foam as a Large Intestinal Delivery Platform for Macromolecules to Treat Inflammatory Bowel Disease. **2024**. DOI: .

(4) Chang, J. T. Pathophysiology of Inflammatory Bowel Diseases. *N. Engl. J. Med.* **2020**, *383* (27), 2652−2664.

(5) Lu, Q.; Yang, M.; Liang, Y.; Xu, J.; Xu, H.; Nie, Y.; Wang, L.; Yao, J.; Li, D. Immunology of Inflammatory Bowel Disease: Molecular Mechanisms and Therapeutics. *J. Inflamm Res.* **2022**, *15*, 1825−1844.
(6) Yang, Y.; Wang, L.; Peugnet-González, I.; Parada-Venegas, D.; Dijkstra, G.; Faber, K. N. cGAS-STING Signaling Pathway in Intestinal Homeostasis and Diseases. *Front. Immunol.* **2023**, *14*, 1239142.
(7) Cai, Z.; Wang, S.; Li, J. Treatment of Inflammatory Bowel Disease: A Comprehensive Review. *Front Med. (Lausanne)* **2021**, *8*, 765474.
(8) Kumar, A.; Smith, P. J. Horizon Scanning: New and Future Therapies in the Management of Inflammatory Bowel Disease. *eGastroenterology* **2023**, *1*, No. e100012.
(9) Saez, A.; Herrero-Fernandez, B.; Gomez-Bris, R.; Sánchez-Martinez, H.; Gonzalez-Granado, J. M. Pathophysiology of Inflammatory Bowel Disease: Innate Immune System. *Int. J. Mol. Sci.* **2023**, *24* (2), 1526.
(10) Decout, A.; Katz, J. D.; Venkatraman, S.; Ablasser, A. The cGAS−STING Pathway as a Therapeutic Target in Inflammatory Diseases. *Nat. Rev. Immunol.* **2021**, *21* (9), 548−569.
(11) Haag, S. M.; Gulen, M. F.; Reymond, L.; Gibelin, A.; Abrami, L.; Decout, A.; Heymann, M.; van der Goot, F. G.; Turcatti, G.; Behrendt, R.; Ablasser, A. Targeting STING with Covalent Small-Molecule Inhibitors. *Nature* **2018**, *559* (7713), 269−273.
(12) Gulen, M. F.; Samson, N.; Keller, A.; Schwabenland, M.; Liu, C.; Glück, S.; Thacker, V. V.; Favre, L.; Mangeat, B.; Kroese, L. J.; Krimpenfort, P.; Prinz, M.; Ablasser, A. cGAS−STING Drives Ageing-Related Inflammation and Neurodegeneration. *Nature* **2023**, *620* (7973), 374−380.
(13) Zhou, J.; Zhuang, Z.; Li, J.; Feng, Z. Significance of the cGAS-STING Pathway in Health and Disease. *Int. J. Mol. Sci.* **2023**, *24* (17), 13316.
(14) Ke, X.; Hu, T.; Jiang, M. cGAS−STING Signaling Pathway in Gastrointestinal Inflammatory Disease and Cancers. *FASEB J.* **2022**, *36* (1), No. e22029.
(15) Uthaman, S.; Parvinroo, S.; Mathew, A. P.; Jia, X.; Hernandez, B.; Proctor, A.; Sajeevan, K. A.; Nenninger, A.; Long, M.-J.; Park, I.-K.; Chowdhury, R.; Phillips, G. J.; Wannemuehler, M. J.; Bardhan, R. Inhibiting the cGAS-STING Pathway in Ulcerative Colitis with Programmable Micelles. *ACS Nano* **2024**, *18* (19), 12117−12133.
(16) Basu, S. M.; Yadava, S. K.; Singh, R.; Giri, J. Lipid Nanocapsules Co-Encapsulating Paclitaxel and Salinomycin for Eradicating Breast Cancer and Cancer Stem Cells. *Colloids Surf., B* **2021**, *204*, 111775.
(17) Groo, A.-C.; Saulnier, P.; Gimel, J.-C.; Gravier, J.; Ailhas, C.; Benoit, J.-P.; Lagarce, F. Fate of Paclitaxel Lipid Nanocapsules in Intestinal Mucus in View of Their Oral Delivery. *Int. J. Nanomedicine* **2013**, *2013*, 4291.
(18) Heurtault, B.; Saulnier, P.; Pech, B.; Proust, J.; Benoit, J.-P. A Novel Phase Inversion-Based Process for the Preparation of Lipid Nanocarriers. *Pharm. Res.* **2002**, *19*, 875−880.
(19) Valsalakumari, R.; Yadava, S. K.; Szwed, M.; Pandya, A. D.; Mælandsmo, G. M.; Torgersen, M. L.; Iversen, T.-G.; Skotland, T.; Sandvig, K.; Giri, J. Mechanism of Cellular Uptake and Cytotoxicity of Paclitaxel Loaded Lipid Nanocapsules in Breast Cancer Cells. *Int. J. Pharm.* **2021**, *597*, 120217.
(20) Lamprecht, A.; Bouligand, Y.; Benoit, J.-P. New Lipid Nanocapsules Exhibit Sustained Release Properties for Amiodarone. *J. Controlled Release* **2002**, *84* (1), 59−68.
(21) Alhouayek, M.; Masquelier, J.; Cani, P. D.; Lambert, D. M.; Muccioli, G. G. Implication of the Anti-Inflammatory Bioactive Lipid Prostaglandin D2-Glycerol Ester in the Control of Macrophage Activation and Inflammation by ABHD6. *Proc. Natl. Acad. Sci. U.S.A.* **2013**, *110* (43), 17558−17563.
(22) Xu, Y.; Van Hul, M.; Suriano, F.; Préat, V.; Cani, P. D.; Beloqui, A. Novel Strategy for Oral Peptide Delivery in Incretin-Based Diabetes Treatment. *Gut* **2020**, *69*, 911−919.
(23) Xu, Y.; Carradori, D.; Alhouayek, M.; Muccioli, G. G.; Cani, P. D.; Préat, V.; Beloqui, A. Size Effect on Lipid Nanocapsule-Mediated GLP-1 Secretion from Enteroendocrine L Cells. *Mol. Pharm.* **2018**, *15*, 108−115.
(24) Schneider, C. A.; Rasband, W. S.; Eliceiri, K. W. NIH Image to ImageJ: 25 Years of Image Analysis. *Nat. Methods* **2012**, *9* (7), 671−675.
(25) Becker, C.; Fantini, M. C.; Neurath, M. F. High Resolution Colonoscopy in Live Mice. *Nat. Protoc.* **2006**, *1* (6), 2900−2904.
(26) Beloqui, A.; Coco, R.; Memvanga, P. B.; Ucakar, B.; des Rieux, A.; Préat, V. PH-Sensitive Nanoparticles for Colonic Delivery of Curcumin in Inflammatory Bowel Disease. *Int. J. Pharm.* **2014**, *473* (1), 203−212.
(27) Beloqui, A.; Coco, R.; Alhouayek, M.; Solinís, M. Á.; Rodríguez-Gascón, A.; Muccioli, G. G.; Préat, V. Budesonide-Loaded Nanostructured Lipid Carriers Reduce Inflammation in Murine DSS-Induced Colitis. *Int. J. Pharm.* **2013**, *454* (2), 775−783.
(28) Koelink, P. J.; Wildenberg, M. E.; Stitt, L. W.; Feagan, B. G.; Koldijk, M.; van 't Wout, A. B.; Atreya, R.; Vieth, M.; Brandse, J. F.; Duijst, S.; te Velde, A. A.; D'Haens, G. R. A. M.; Levesque, B. G.; van den Brink, G. R. Development of Reliable, Valid and Responsive Scoring Systems for Endoscopy and Histology in Animal Models for Inflammatory Bowel Disease. *Journal of Crohn's and Colitis* **2018**, *12* (7), 794−803.
(29) Zhang, S.; Zheng, R.; Pan, Y.; Sun, H. Potential Therapeutic Value of the STING Inhibitors. *Molecules* **2023**, *28* (7), 3127.
(30) Hong, Z.; Mei, J.; Li, C.; Bai, G.; Maimaiti, M.; Hu, H.; Yu, W.; Sun, L.; Zhang, L.; Cheng, D.; Liao, Y.; Li, S.; You, Y.; Sun, H.; Huang, J.; Liu, X.; Lieberman, J.; Wang, C. STING Inhibitors Target the Cyclic Dinucleotide Binding Pocket. *Proc. Natl. Acad. Sci. U.S.A.* **2021**, *118* (24), No. e2105465118.
(31) Kobritz, M.; Borjas, T.; Patel, V.; Coppa, G.; Aziz, M.; Wang, P. H151, a small molecule inhibitor of STING as a novel therapeutic in intestinal ischemia-reperfusion injury. *Shock* **2022**, *58* (3), 241−250.
(32) Ou, L.; Zhang, A.; Cheng, Y.; Chen, Y. The cGAS-STING Pathway: A Promising Immunotherapy Target. *Front Immunol* **2021**, *12*, 795048.
(33) Alagga, A. A.; Pellegrini, M. V.; Gupta, V. *Drug Absorption. In StatPearls*; StatPearls Publishing: Treasure Island (FL), 2024.
(34) Souza, R. F.; Caetano, M. A. F.; Magalhães, H. I. R.; Castelucci, P. Study of Tumor Necrosis Factor Receptor in the Inflammatory Bowel Disease. *World J. Gastroenterol* **2023**, *29* (18), 2733−2746.
(35) Andreou, N.-P.; Legaki, E.; Gazouli, M. Inflammatory Bowel Disease Pathobiology: The Role of the Interferon Signature. *Ann. Gastroenterol* **2020**, *33* (2), 125−133.
(36) Shi, Z.; Shen, J.; Qiu, J.; Zhao, Q.; Hua, K.; Wang, H. CXCL10 Potentiates Immune Checkpoint Blockade Therapy in Homologous Recombination-Deficient Tumors. *Theranostics* **2021**, *11* (15), 7175−7187.
(37) Guo, S.; Al-Sadi, R.; Said, H. M.; Ma, T. Y. Lipopolysaccharide Causes an Increase in Intestinal Tight Junction Permeability *in Vitro* and *in Vivo* by Inducing Enterocyte Membrane Expression and Localization of TLR-4 and CD14. *Am. J. Pathol.* **2013**, *182* (2), 375−387.
(38) Dabholkar, N.; Waghule, T.; Krishna Rapalli, V.; Gorantla, S.; Alexander, A.; Narayan Saha, R.; Singhvi, G. Lipid Shell Lipid Nanocapsules as Smart Generation Lipid Nanocarriers. *J. Mol. Liq.* **2021**, *339*, 117145.
(39) Plaza-Oliver, M.; Santander-Ortega, M. J.; Lozano, M. V. Current Approaches in Lipid-Based Nanocarriers for Oral Drug Delivery. *Drug Deliv. Transl. Res.* **2021**, *11* (2), 471−497.
(40) Porter, C. J. H.; Trevaskis, N. L.; Charman, W. N. Lipids and Lipid-Based Formulations: Optimizing the Oral Delivery of Lipophilic Drugs. *Nat. Rev. Drug Discov* **2007**, *6* (3), 231−248.
(41) Drucker, D. J. Glucagon-Like Peptide 2. *Journal of Clinical Endocrinology & Metabolism* **2001**, *86* (4), 1759−1764.
(42) Ren, W.; Wu, J.; Li, L.; Lu, Y.; Shao, Y.; Qi, Y.; Xu, B.; He, Y.; Hu, Y. Glucagon-Like Peptide-2 Improve Intestinal Mucosal Barrier Function in Aged Rats. *Journal of nutrition, health and aging* **2018**, *22* (6), 731−738.

https://doi.org/10.1021/acs.molpharmaceut.4c01297
Mol. Pharmaceutics 2025, 22, 2108−2121

(43) Mehta, M.; Bui, T. A.; Yang, X.; Aksoy, Y.; Goldys, E. M.; Deng, W. Lipid-Based Nanoparticles for Drug/Gene Delivery: An Overview of the Production Techniques and Difficulties Encountered in Their Industrial Development. *ACS Mater. Au* **2023**, *3* (6), 600−619.
(44) Xu, L.; Wang, X.; Liu, Y.; Yang, G.; Falconer, R. J.; Zhao, C.-X. Lipid Nanoparticles for Drug Delivery. *Advanced NanoBiomed Research* **2022**, *2* (2), 2100109.
(45) Seo, Y.; Lim, H.; Park, H.; Yu, J.; An, J.; Yoo, H. Y.; Lee, T. Recent Progress of Lipid Nanoparticles-Based Lipophilic Drug Delivery: Focus on Surface Modifications. *Pharmaceutics* **2023**, *15* (3), 772.
(46) Richter, M.; Piwocka, O.; Musielak, M.; Piotrowski, I.; Suchorska, W. M.; Trzeciak, T. From Donor to the Lab: A Fascinating Journey of Primary Cell Lines. *Front. Cell Dev. Biol.* **2021**, *9*, 711381.
(47) Pan, J.; Fei, C.-J.; Hu, Y.; Wu, X.-Y.; Nie, L.; Chen, J. Current Understanding of the cGAS-STING Signaling Pathway: Structure, Regulatory Mechanisms, and Related Diseases. *Zool Res.* **2023**, *44* (1), 183−218.
(48) Chassaing, B.; Aitken, J. D.; Malleshappa, M.; Vijay-Kumar, M. Dextran Sulfate Sodium (DSS)-Induced Colitis in Mice. *Curr. Protoc Immunol* **2014**, *104*, 15.25.1.
(49) Yang, C.; Merlin, D. Unveiling Colitis: A Journey through the Dextran Sodium Sulfate-Induced Model. *Inflammatory Bowel Diseases* **2024**, *30* (5), 844−853.
(50) Hu, Z.; Zhang, F.; Brenner, M.; Jacob, A.; Wang, P. The Protective Effect of H-151, a Novel STING Inhibitor, in Renal Ischemia-Reperfusion-Induced Acute Kidney Injury. *American Journal of Physiology-Renal Physiology* **2023**, *324* (6), F558−F567.
(51) Gong, W.; Lu, L.; Y, Z.; Zhou, Y.; Ma, H.; Fu, L.; Huang, S.; Y, Z.; Zhang, A.; Jia, Z. The Novel STING Antagonist H-151 Ameliorates Cisplatin-Induced Acute Kidney Injury and Mitochondrial Dysfunction. *Am J Physiol Renal Physiol* **2021**, *320*, F608−F616.
(52) Hu, S.; Gao, Y.; Gao, R.; Wang, Y.; Qu, Y.; Yang, J.; Wei, X.; Zhang, F.; Ge, J. The Selective STING Inhibitor H-151 Preserves Myocardial Function and Ameliorates Cardiac Fibrosis in Murine Myocardial Infarction. *Int. Immunopharmacol.* **2022**, *107*, 108658.
(53) Lockhart, J. S.; Sumagin, R. Non-Canonical Functions of Myeloperoxidase in Immune Regulation, Tissue Inflammation and Cancer. *Int. J. Mol. Sci.* **2022**, *23* (20), 12250.
(54) Rizo-Téllez, S. A.; Sekheri, M.; Filep, J. G. Myeloperoxidase: Regulation of Neutrophil Function and Target for Therapy. *Antioxidants* **2022**, *11* (11), 2302.
(55) Lin, W.; Chen, H.; Chen, X.; Guo, C. The Roles of Neutrophil-Derived Myeloperoxidase (MPO) in Diseases: The New Progress. *Antioxidants* **2024**, *13* (1), 132.
(56) Wéra, O.; Lancellotti, P.; Oury, C. The Dual Role of Neutrophils in Inflammatory Bowel Diseases. *J. Clin Med.* **2016**, *5* (12), 118.

https://doi.org/10.1021/acs.molpharmaceut.4c01297
Mol. Pharmaceutics 2025, 22, 2108−2121